# Electronic supplementary information

## Hierarchically structured C@$SnO_2$@C nanofiber bundles with high stability and effective ambipolar diffusion kinetics for high-performance Li-ion batteries

Xiaoling Wang,[a] Jingze Li,[a] Zeui Chen,[b] Lijie Lei,[b] Xuepin Liao,[a] Xin Huang[a,b*] and Bi Shi[b]

[a] Department of Biomass Chemistry and Engineering, Sichuan University, Chengdu 610065, China. Email: xhuangscu@163.com

[b] National Engineering Laboratory for Clear Technology of Leather Manufacture, Sichuan University, Chengdu 610065, China

*Correspondence - xhuangscu@163.com

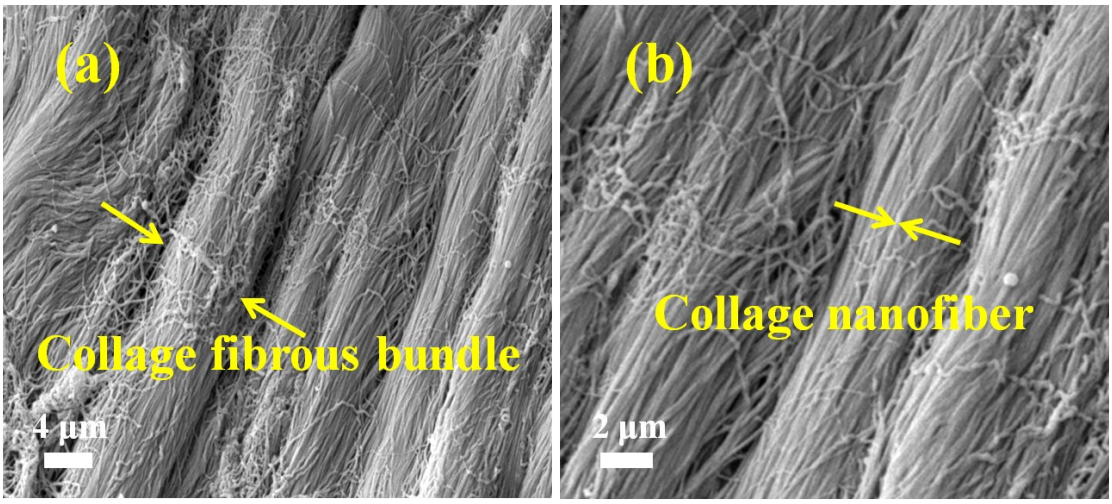


**Fig. S1.** SEM images of CF at different magnifications.

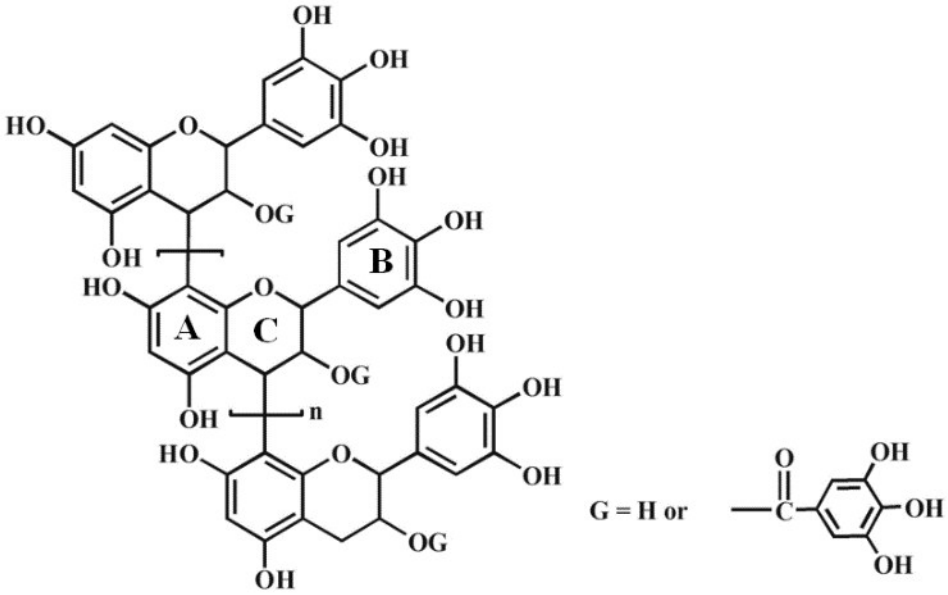


**Fig. S2.** Molecular structure of bayberry tannin (BT). BT contains abundant hydrophilic hydroxyl groups and hydrophobic aromatic backbone, which can be coated onto CF through hydrogen-bonding and hydrophobic interactions.[1-3]

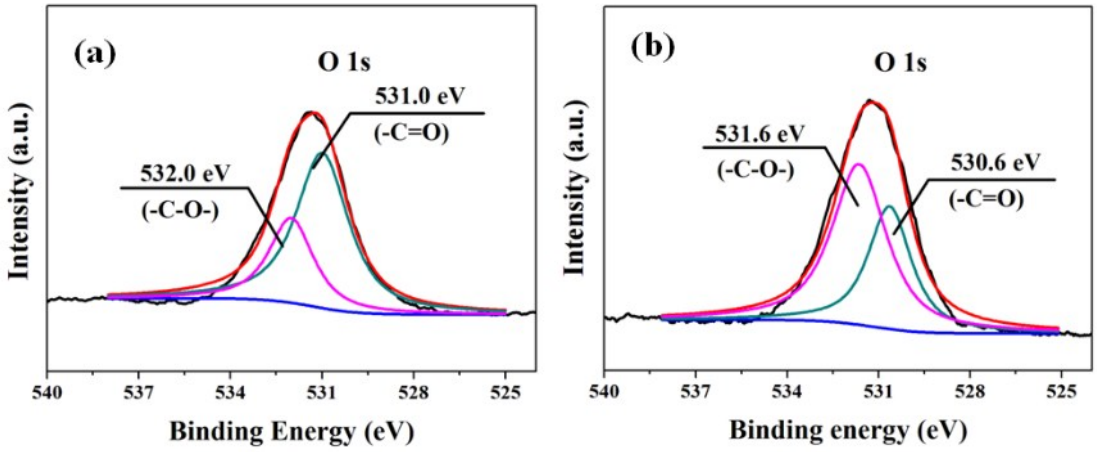


**Fig. S3.** The O 1s X-ray photoelectron spectra (XPS) of (a) CF and (b) CF@$Sn^{4+}$. In Fig. S3a, the peaks at 532.0 eV and 531.0 eV are attributed to -C-O and -C=O groups of CF.[4] After CF was reacted with $Sn^{4+}$ (Fig. S3b), the peak intensity of -C-O is substantially increased along with significant decreased peak intensity of -C=O. These changes suggest that CF should be mainly chelated with $Sn^{4+}$ via its -COOH groups.

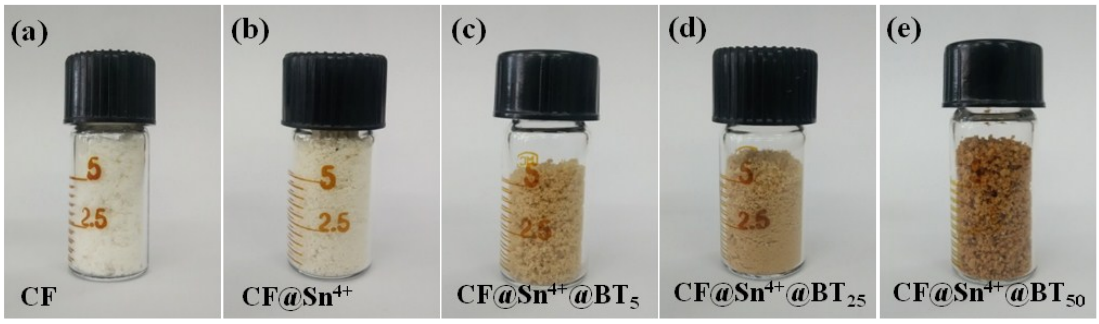


**Fig. S4.** Digital images of (a) CF, (b) CF@$Sn^{4+}$, (c) CF@$Sn^{4+}$@$BT_5$, (d) CF@$Sn^{4+}$@$BT_{25}$ and (e) CF@$Sn^{4+}$@$BT_{50}$.

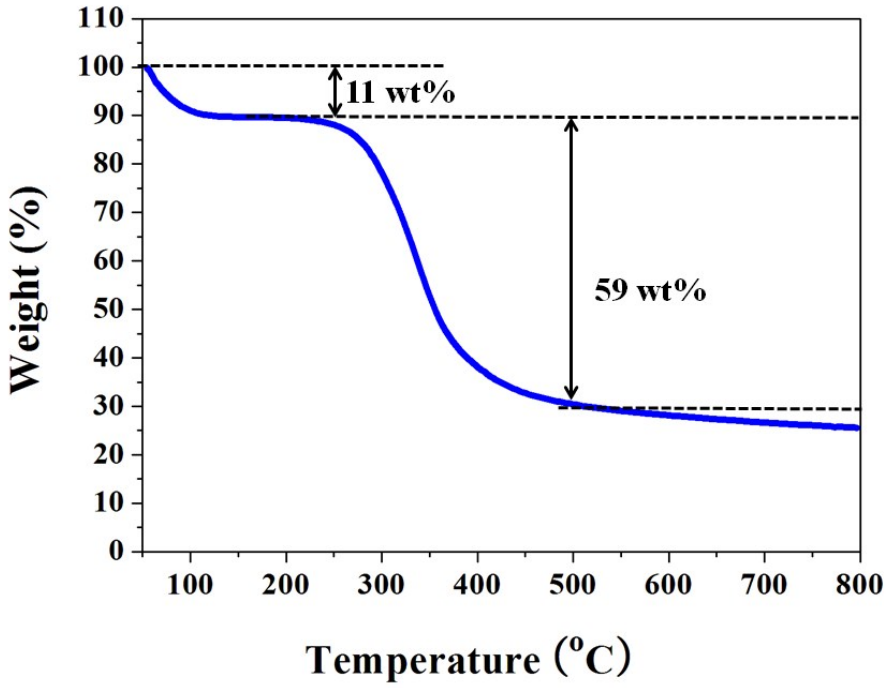


**Fig. S5.** Thermogravimetry analysis (TGA) of CF in nitrogen atmosphere with a heating rate of 10 °C $min^{-1}$. The TGA curve shows two steps of weight loss below 500 °C. The first step of weight loss below 150 °C is associated with the loss of adsorbed water on CF, and the second step of weight loss is due to the decomposition of collagen protein in the temperature range of 250-500 °C.

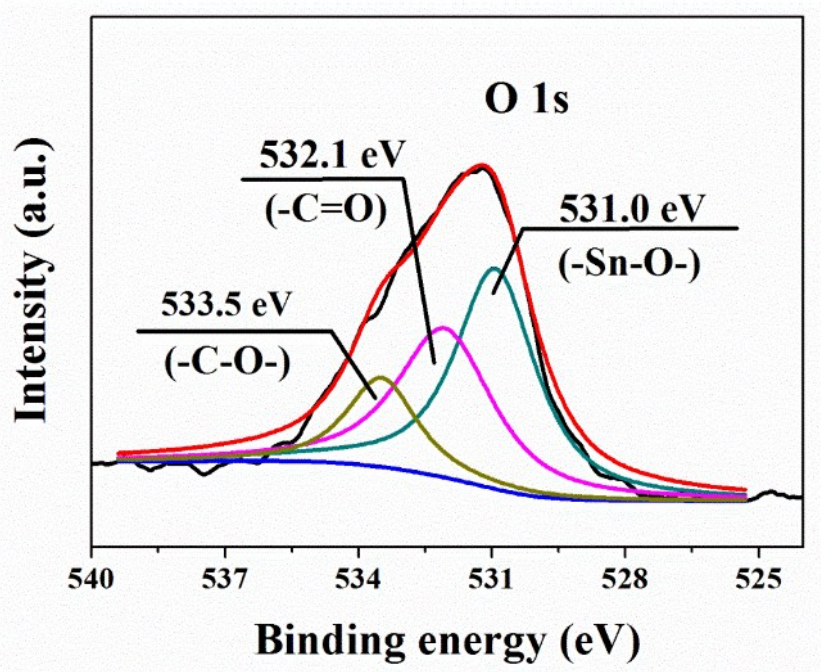


**Fig. S6.** The O 1s XPS of C@$SnO_2$@C. The spectra consist of three peaks at 533.5 eV, 532.1 eV and 530.9 eV, which are attributed to -C-O, -C=O and -Sn-O-, respectively. The peak of -Sn-O- is ascribed to the existing of $SnO_2$, while the presence of -C-O and -C=O suggests that carboxyl group and hydroxyl group still exist in C@$SnO_2$@C, which are responsible for the stabilization of $SnO_2$ nanoparticles on C@$SnO_2$@C.

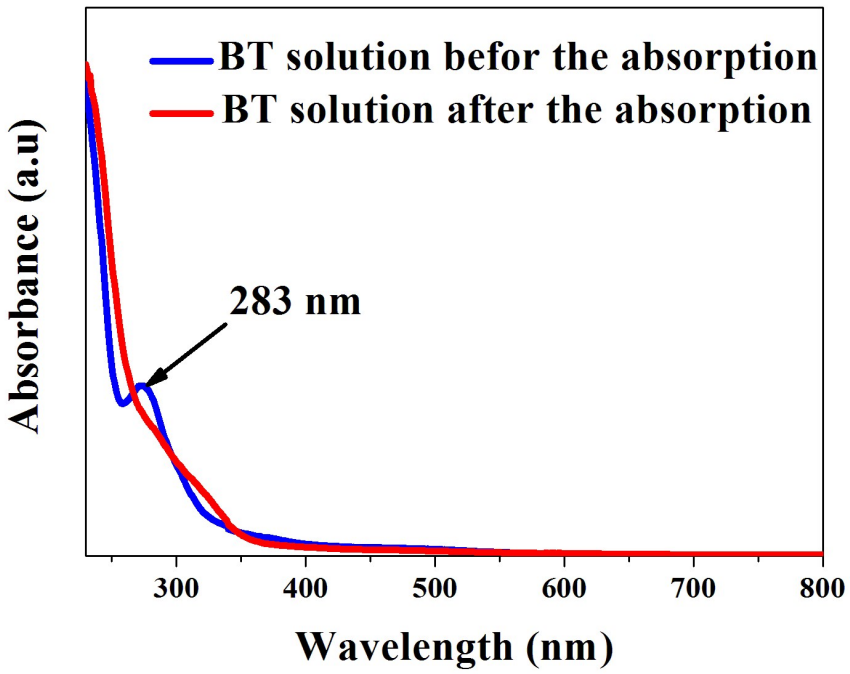


**Fig. S7.** UV-vis absorption spectra of BT solution before and after the adsorption by $SnO_2$ nanofiber bundle. Before the adsoprtion, BT showed a major peak around 283 nm, which disappeared after the adsorption of $SnO_2$, confirming the successful coating of BT onto $SnO_2$ nanofiber bundle.

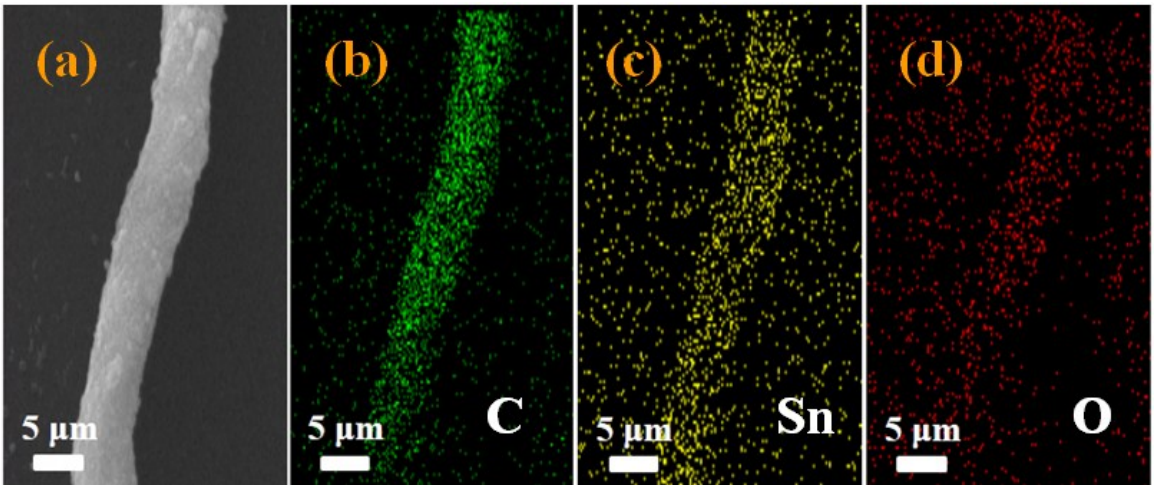


**Fig. S8.** SEM-EDS mapping images of C, Sn, O in C@$SnO_2$@C.

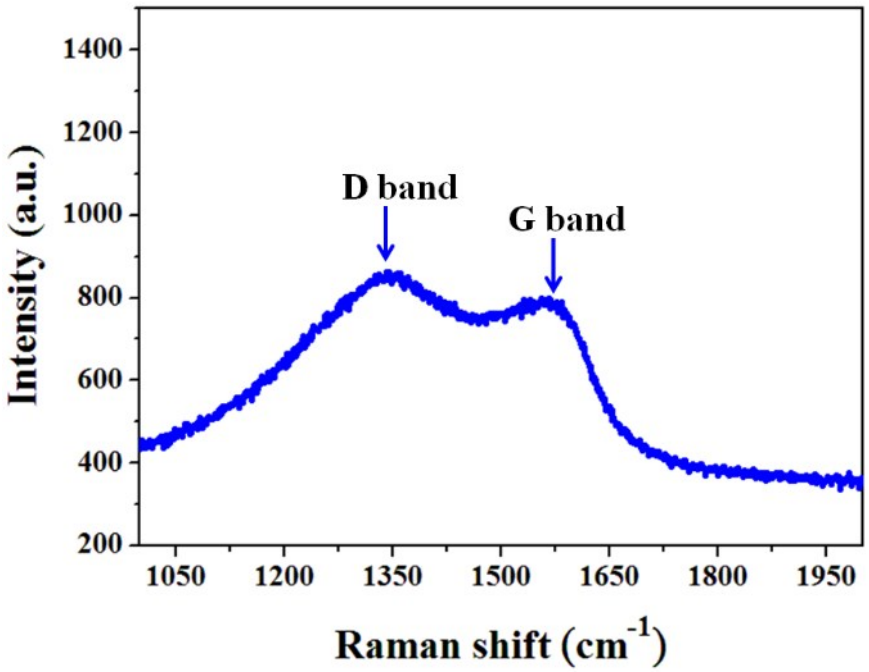


**Fig. S9.** Raman spectrum of C@$SnO_2$@C.

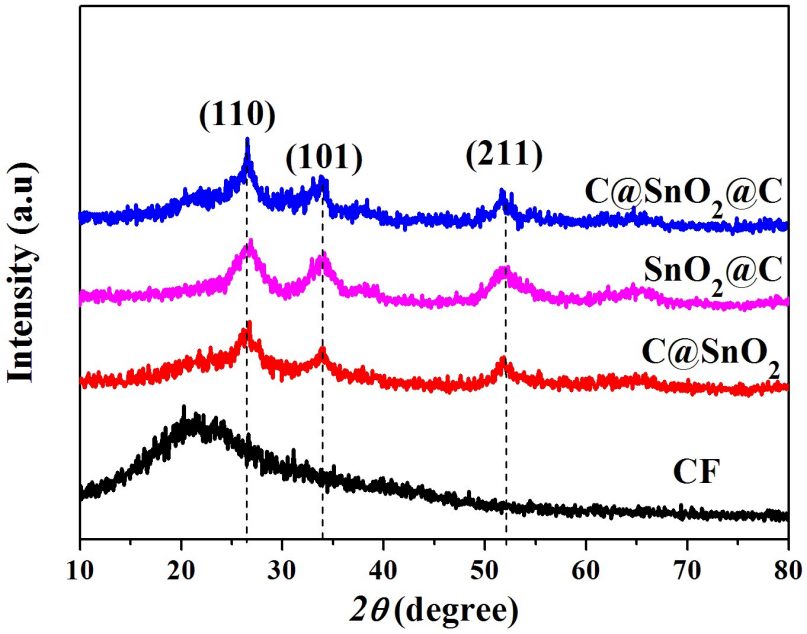


**Fig. S10.** X-ray diffraction (XRD) patterns of CF, C@$SnO_2$@C, C@$SnO_2$ and $SnO_2$@C. XRD pattern of CF shows one broad characteristic peak at 23º, which is attributed to the amorphous polymer phase of CF. XRD patterns of C@$SnO_2$@C, C@$SnO_2$ and $SnO_2$@C exhibit typical (110), (101) and (211) crystalline plane diffraction peaks of face-centered-cubic (*fcc*) $SnO_2$ at 26.6º, 33.8º and 52.3º, respectively.[5]

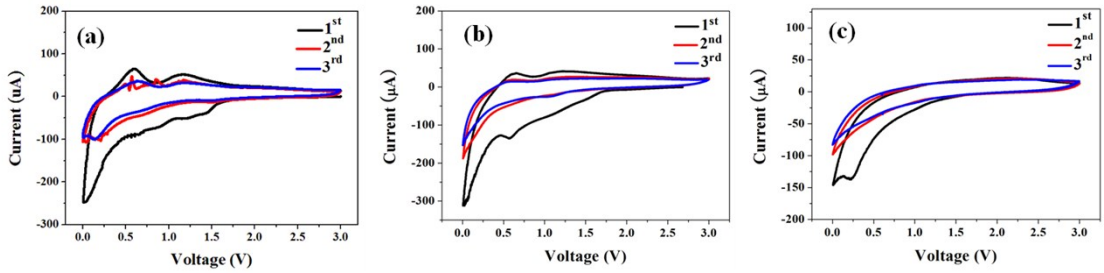


**Fig. S11.** Initial three cyclic voltammograms (CV) of C@$SnO_2$@C (a), C@$SnO_2$ (b) and $SnO_2$@C (c) at a scan rate of 0.05 mV $s^{-1}$.

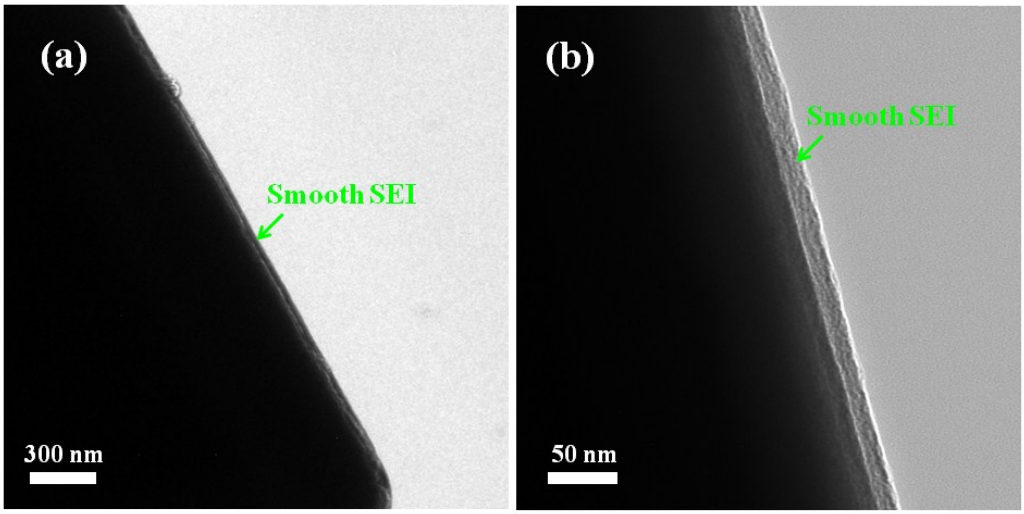


**Fig. S12.** TEM images of C@$SnO_2$@C after the rate tests.

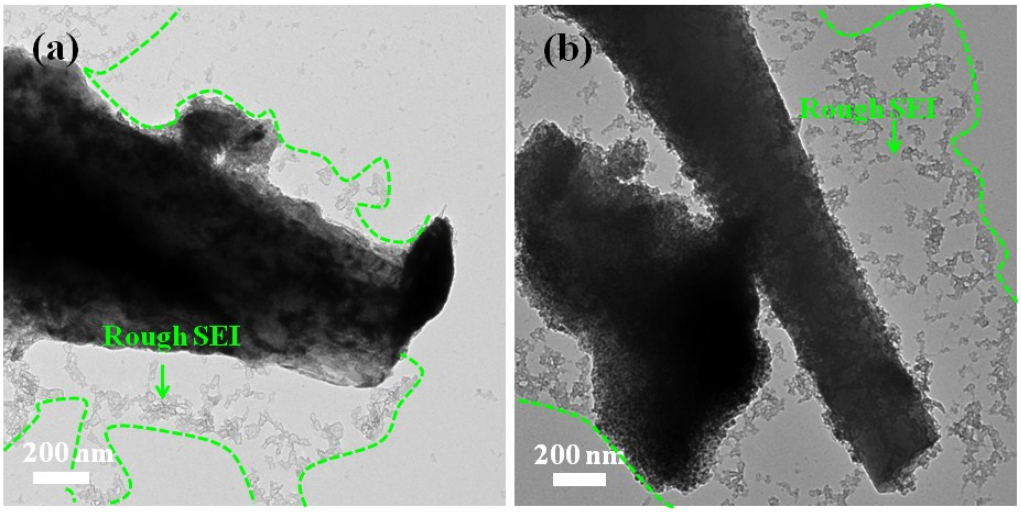


**Fig. S13.** TEM images of C@$SnO_2$ after the rate tests.

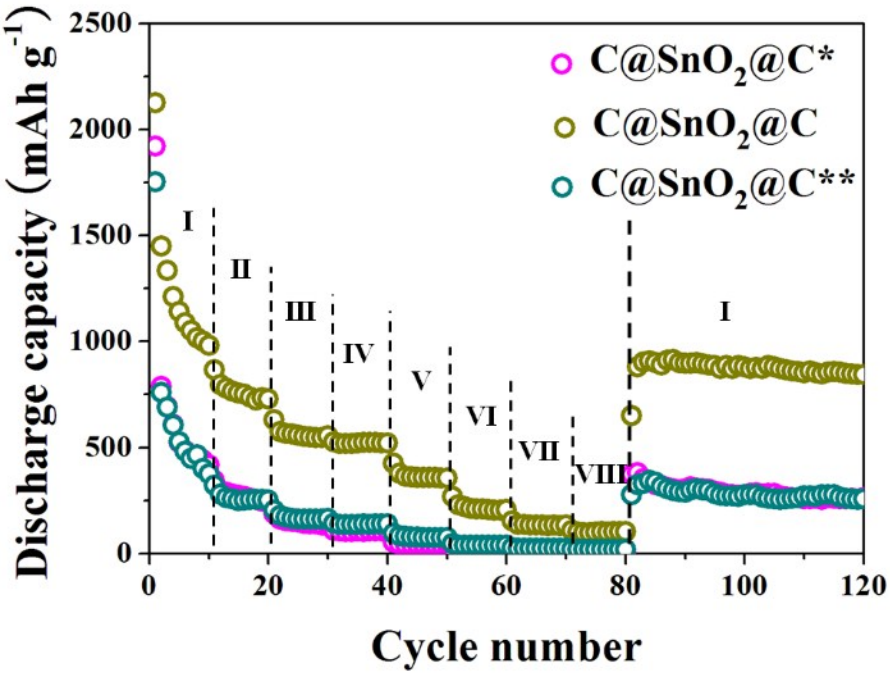


**Fig. S14.** Rate capabilities of C@$SnO_2$@C*, C@$SnO_2$@C and C@$SnO_2$@C**. The current density at each stage: I = 0.2 A $g^{-1}$, II = 0.4 A $g^{-1}$, III = 0.8 A $g^{-1}$, IV = 1.0 A $g^{-1}$, V = 2.0 A $g^{-1}$, VI = 4.0 A $g^{-1}$, VII = 6.0 A $g^{-1}$, VIII = 8.0 A $g^{-1}$.

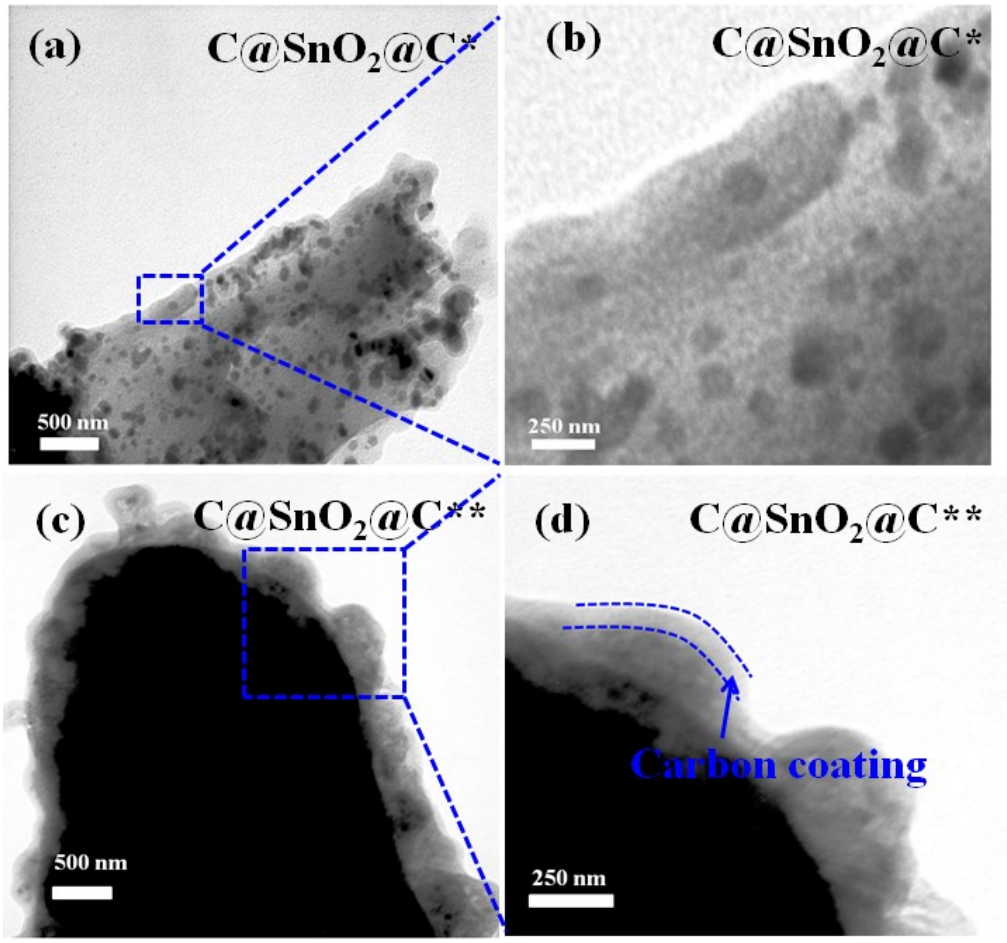


**Fig. S15.** TEM images of (a, b) C@$SnO_2$@C* and (c, d) C@$SnO_2$@C**.

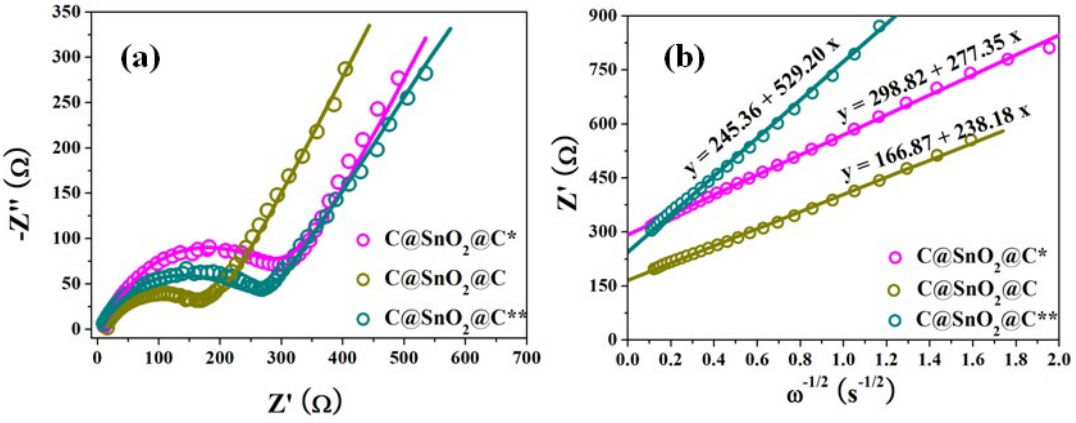


**Fig. S16.** (a) EIS of C@$SnO_2$@C*, C@$SnO_2$@C and C@$SnO_2$@C** after the rate tests and (b) the corresponding relationship between $Z'$ and $\omega^{-1/2}$ in the low-frequency region.

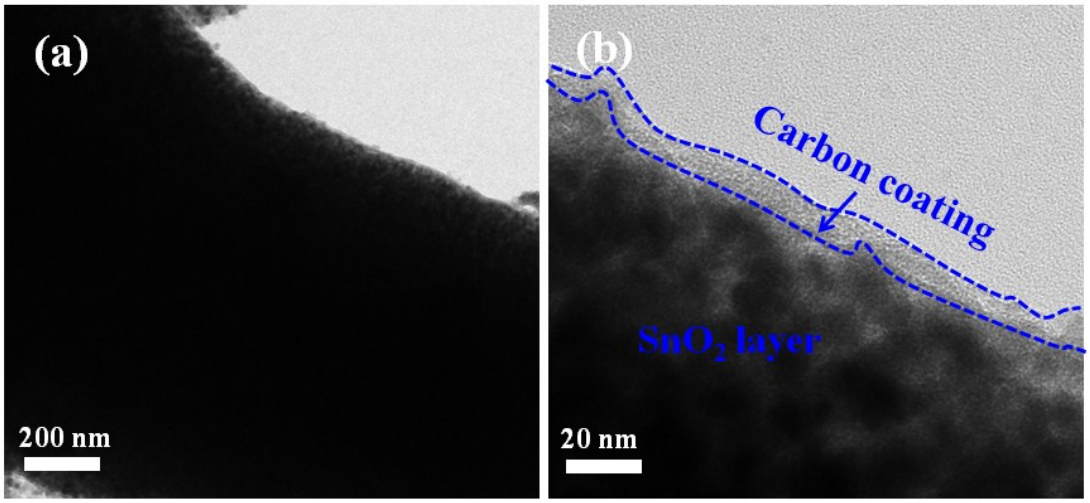


**Fig. S17.** TEM images of $SnO_2$@C at different magnifications.

**Table S1.** EIS parameters obtained by fitting the Nyquist plots of C@$SnO_2$@C, C@$SnO_2$@C* and C@$SnO_2$@C** after the rate tests using the equivalent electrical circuit model.

| Sample | $R_{ct}$ (Ω) | $Z_w$ (Ω) |
|---|---|---|
| C@$SnO_2$@C | 167.2 | 150.6 |
| C@$SnO_2$@C * | 309.4 | 289.6 |
| C@$SnO_2$@C** | 260.1 | 486.3 |

**Table S2.** Discharge capacity of various carbon/$SnO_2$ nanocomposites.

| Sample | Discharge capacity (mAh $g^{-1}$) | Current density (mA $g^{-1}$) | Cycle number | Reference |
|---|---|---|---|---|
| C@$SnO_2$@C nanofiber bundle | 500 | 500 | 100 | This work |
| $SnO_2$@carbon hollow nanospheres | 460 | 500 | 100 | 6 |
| CNFs@$SnO_2$ core-shell structures | 460 | 200 | 50 | 7 |
| Mesoporous $SnO_2$ overlaying MWCNTs hybrid composites | 344.5 | 33.3 | 50 | 8 |
| $SnO_2$@carbon nanofibers | 420 | 100 | 100 | 9 |
| CNTs/mesoporous $SnO_2$ | 464 | 626 | 40 | 10 |
| $SnO_2$/carbon hollow spheres | 473 | 100 | 50 | 11 |
| Carbon-coated $SnO_2$ nanocolloids | 440 | 300 | 100 | 12 |

**Table S3.** EIS parameters obtained by fitting the Nyquist plots of C@$SnO_2$@C, C@$SnO_2$ and $SnO_2$@C before and after cycled at 0.5 A $g^{-1}$ and 1.0 A $g^{-1}$ using the equivalent electrical circuit model.

| | C@$SnO_2$@C | C@$SnO_2$ | $SnO_2$@C |
|---|---|---|---|
| $R_{ct}$ (Ω) | 201.3[a] (168.4[b]/27.2[c]) | 108.1 (112.3/25.0) | 79.1 (103.6/70.3) |
| $Z_w$ (Ω) | 180.1[a] (143.6[b]/94.2[c]) | 158.2 (179.7/218.5) | 350.6 (278.7/193.0) |

[a] Parameters obtained by fitting the Nyquist plots of electrode materials before the rate tests.

[b] Parameters obtained by fitting the Nyquist plots of electrode materials after cycled at 0.5 A $g^{-1}$.

[c] Parameters obtained by fitting the Nyquist plots of electrode materials after cycled at 1.0 A $g^{-1}$.

## References


1. T. Okuda and H. Ito, *Molecules*, 2011, **16**, 2191-2217.
2. X. Huang, H. Wu, X. P. Liao and B. Shi, *Green Chem.*, 2010, **12**, 395-399.
3. I. Mueller-Harvey, *Anim. Feed Sci. Technol.*, 2001, **91**, 3-20.
4. N. A. Evans, B. Miligan and K. C. Montgomery, *J. Am. Leather Chem. Assoc.*, 1987, **82**, 86-95.
5. J. X. Wang, W. Li, F. Wang, Y. Y. Xia, A. M. Asiriand and D. Y. Zhao, *Nanoscale*, 2014, **6**, 3217-3222.
6. X. W. Lou, C. M. Li and L. A. Archer, *Adv. Mater.*, 2009, **21**, 2536-2539.
7. L. Zhang, G. Q. Zhang, H. B. Wu, L. Yu and X. W. Luo, *Adv. Mater.*, 2013, **25**, 2589-2593.
8. Z. H. Wen, Q. Wang, Q. Zhang and J. H. Li, *Adv. Funct. Mater.*, 2007, **17**, 2772-2778.
9. Z. X. Yang, G. D. Du, Z. P. Guo, X. B. Yu, Z. X. Chen, P. Zhang, G. N. Chen and H. K. Liu, *J. Mater. Res.*, 2010, **25**, 1516-1524.
10. G. Chen, Z. Y. Wang and D. G. Xia, *Chem. Mater.*, 2008, **20**, 6951-6956.
11. X. W. Lou, D. Deng, J. Y. Lee and L. A. Archer, *Chem. Mater.*, 2008, **20**, 6562-6566.
12. X. W. Lou, J. S. Chen, P. Chen and L. A. Archer, *Chem. Mater.*, 2009, **21**, 2868-2874.